-RESEARCH PAPER-

International Journal of Mining and Geo-Engineering

IJMGE

IJMGE 58-4 (2024) 327-339

DOI: 10.22059/IJMGE.2024.376761.595167

The application of an improved artificial neural network model for prediction of Cu and Au concentration in the porphyry copper-epithermal gold deposits, case study: Masjed Daghi, NW Iran

Habibollah Bazdar [a], Ali Imamalipour [a, *]

[a] *Department of Mining Engineering, Faculty of Engineering, Urmia University, Urmia, Iran.*

Article History:

Received: 24 May 2024.

Revised: 18 July 2024.

Accepted: 18 August 2024.

ABSTRACT

Modelling of geochemical data to predict elements is done using different methods. The proposed method in this research is the use of an intelligent model and pathfinder elements. In this study, drilling and sampling were conducted in two porphyry and epithermal mineralization of the Masjed Daghi porphyry copper deposit. We used the data from the porphyry mineralization to predict copper and the data from the epithermal mineralization to predict gold. By geochemical data and performing correlation and sensitivity analyses, copper and gold pathfinder elements (Pb, Zn, Ag, Mo, and As) were determined. Then, using the data of pathfinder elements and an intelligent artificial neural network model, we predict the grade of gold and copper elements. The data of pathfinder elements were used as input and the grade of gold and copper elements were used as the output of the model. In this research, the optimization of the artificial neural network (ANN) is accomplished using several optimization algorithms, such as the simulated annealing algorithm (SAA), firefly algorithm (FA), invasive weed optimization algorithm (IWO), and shuffled frog leaping algorithm (SFLA). Comparing the results showed that the ANN-SAA (Combining ANN with SAA) performs better than other built models. This superiority was evident in both the porphyry and epithermal mineralization. The R^2 and MSE of the ANN-SAA model for Cu prediction were 0.8275 and 0.0303 for the training data, 0.7357 and 0.0371 for the testing data, respectively. Also, the R^2 and MSE of the ANN-SAA model for Au prediction were 0.6713 and 0.0463 for the training data, 0.7040 and 0.0333 for the testing data, respectively.

Keywords: *Prediction of Cu and Au, Artificial neural network, Evolutionary algorithms, Arasbaran metallurgical zone, Porphyry copper deposits.*

1. Introduction

Ore grade estimation is one of the most critical issues in the exploration of any mineral deposit. The effect of the accuracy of ore grade estimation is continuously related to mining projects from beginning to end. The most common exploratory operation that definitively determines the presence or absence of mineralization is exploratory drilling. However, creating a model that will solve our need for extensive excavations will be very effective in the economic justification of exploration operations. This model can provide a general prediction of the possible distribution of minerals in the studied area. In this context, statistical methods, such as kriging interpolation [1-4], the weight of evidence [5, 6], fuzzy approaches [7, 8], fractal method [9-11] Bayesian methods [12, 13], and integrated methods in the analysis of geochemical data [14-17] have been used. Soft computing is also used as a novel modelling method in exploration projects. For example, artificial neural network (ANN) is used for gold MPM [18-29] and the estimation of gold grade [30-33]. Other intelligent methods, such as support vector machine (SVM) [34-37], Hybrid Machine learning technique [38], neural fuzzy [39, 40] are also used to estimate MPM, gold grade, and related elements.

Over the past years, the use of intelligent methods, including ANNs, has rapidly developed in various fields. This development is due to the good performance and ability of intelligent methods to solve complex non-linear problems. Normally, in non-linear problems, the relationship between the input and output of the system is complicated. The ANN has a high ability to solve such problems; for this reason, its application has expanded [41].

The main goal of this study is to build a model to solve a non-linear problem in the geosciences and geochemical data. Also, optimizing the ANN model, which includes determining the weights and biases of the model, is one of the main approaches of this article. Conventionally, the ANN is optimized by the back propagation (BP) algorithm, which has problems, such as getting stuck in the local minimum and overfitting. Optimization algorithms are superior in terms of exploration and exploitation, so they do not have the problem of falling into local minima. [42-44].

Various studies related to applying evolutionary algorithms, such as particle swarm optimization [45] and genetic algorithm [46] have been used to optimize the ANN model.

In this study, the proposed method is to use the optimal ANN model for ore grade estimation. The implementation of optimization increases the efficiency of the ANN model. Four optimization algorithms (SAA, FA, IWO, and SFLA) were used to determine the parameters of the ANN model. In the end, by comparing the results, the best-built model was selected.

* Corresponding author. *Tel:* +984432752741-43, *E-mail address:* a.imamalipour@urmia.ac.ir (A. Imamalipour).

2. Case Study

2.1. Geological setting

The Arasbaran district is located in the northwest of Iran, in the East Azerbaijan and Ardabil provinces. This zone is the southern continuation of the Lesser Caucasus metallogenic and volcano-plutonic belt [47-50]. The Arasbaran metallurgical zone is situated in the western end of the Alborz-Azerbaijan magmatic arc and the northern extension of the Urmia-Dokhtar magmatic arc (Fig. 1). Its importance is due to the presence of copper-molybdenum porphyry deposits, such as Songun, Sunajil, Haft Cheshme, Farmaza, and Anjard deposits. Similarly, it is an epithermal gold deposit (Fig. 2). Geochemical exploration and field surveys by the Geological Survey and Mineral Exploration of Iran (GSMEI) led to the discovery of several epithermal gold deposits, including Sharafabad, Safi Khanlu, Zaglik, Masjed Daghi and copper-molybdenum-gold in Qara Chiller.

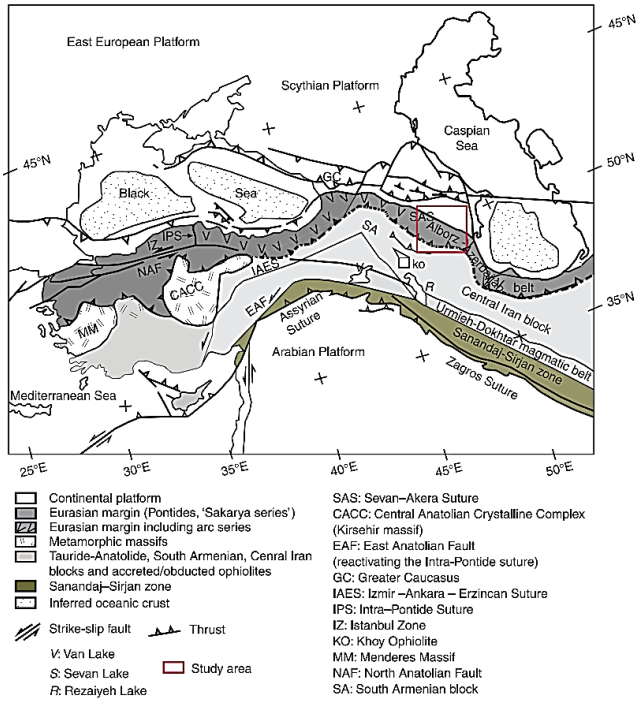

Fig 1. Tectonic map of the Tethyan belt extending from Turkey to Central Iran, showing major tectonic units, suture zones, faults, and plate boundaries [49].

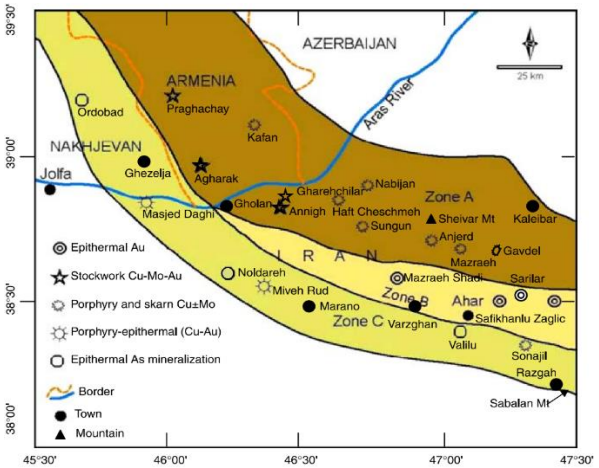

Fig. 2: Distribution map of main Cu-Mo-Au deposits in northwestern Iran and eastern Armenia [49].

2.2. Masjed Daghi Cu-Au porphyry deposit

The Masjed Daghi deposit is located in the province of East Azarbayjan, in the vicinity of the Aras River, and it is a part of the Jolfa sheet (1:100,000 series), with an area of about 8 km^2. The major and oldest lithological units of this area include a collection of flysch and limestone rocks that were deposited in a Mesozoic-Cenozoic sedimentary basin (Fig. 3). This sedimentary complex has been intruded by volcanic and sub-volcanic rocks, including andesite, trachyte-andesite, and diorite. [51]. The most important plutonic event in the area, which is mostly associated with metal mineralization, is the Qara Dagh intrusive igneous body. Several mineralization (copper, gold, and molybdenum porphyry) related to this body are known and are being exploited on the other bank of the Aras River in Armenia and Azerbaijan (Fig. 2).

2.3. Types of mineralization

A variety of mineralization is seen in the Masjed Daghi area, which includes porphyry copper (gold) and epithermal gold mineralization. So, the Masjed Daghi deposit is a porphyry system.

2.3.1. Copper porphyry mineralization

This mineralization has a relatively limited outcrop and can be seen as zones of about 100 m^2 on the surface. The host of porphyry mineralization is an intrusive igneous body with a diorite composition (hornblende-biotite diorite porphyry), which has a small surface outcrop. But the drilling carried out shows the extension of the said body in depth. The mineralogy includes pyrite, chalcopyrite, bornite, and magnetite with small amounts of molybdenite accompanying potassic alteration. The presence of hypogene mineral complexes with potassium alteration is one of the characteristics of copper porphyry mineralization and there is a high possibility that the mineral occurrence of Masjed Daghi does not have an economic value as a supergene enrichment zone. The grade of Cu in porphyry-type mineralization varies between 0.25% and 0.65%. In some samples, the grade of Cu has been measured at up to 1%. Considering the total reserve of Masjed Daghi, the average grades of Cu and Mo are 0.27 wt% and 0.006 wt%, respectively, and the total ore reserve is 340 million metric tons (Mt) [47].

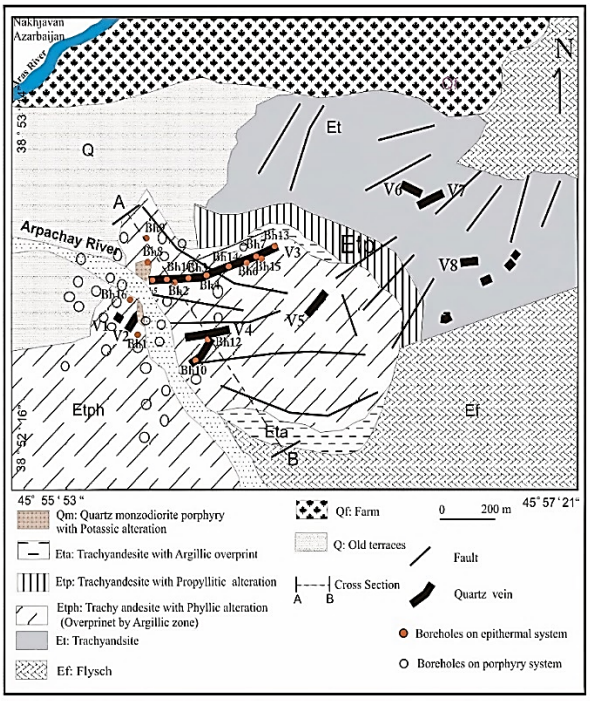

Fig. 3: The geological map in the study area [52].

2.3.2. Epithermal gold mineralization

This type of mineralization has the largest outcrop compared to other mineralization and its area is at least 1 km^2. The mineralization can be seen in the form of silicified rocks, quartz veins, and silica stockworks of various thicknesses and lengths. The mineralogy of this mineralization is generally quartz ± barite with very little sulfides. The main vein in the exploration area is V_3, which is about 700 m long and has an average thickness of 5 m. The dip of the vein is 70 degrees to the south, and its strike is east-west. The V_4 vein is the second major vein, which is about 600 m long and its thickness varies between 2 and 3 m. Based on the analysis results, the Au grade has been measured at up to 5 ppm (the main vein is 2 ppm). The ore reserve of the main vein is 600,000 metric tons [51].

2.4. Alterations of Masjed Daghi deposit

Alteration in the Masjed Daghi has a widespread and also various alteration types can be distinguished. In this section, the types of alterations known using mineralogical studies and their maps are presented.

2.4.1. Potassic alteration

Potassic alteration can be seen in the Masjed Daghi region along the eastern and western banks of the Arpachai seasonal river. This alteration has a limited outcrop (about 100 square meters) and has been widely affected by secondary alterations (phyllic and argillic). The mineralogy of this alteration is an indicator of porphyry systems and includes potassium feldspar (orthoclase), biotite, and magnetite. The formation of pink orthoclase along the seams is quite clear and indicates the secondary origin of this mineral. Biotite is observed as fracture filling and in some cases, its volume in the sample reaches several percent. In most of the samples, magnetite has been transformed into hematite due to the influence of delayed changes. Drilling has shown that this alteration is associated with copper mineralization and continues up to 200 meters. Due to the weathering of copper sulfides and the formation of secondary minerals, such as malachite, the color of this alteration is often green.

2.4.2. Phyllic alteration

This alteration has spread a lot in the Masjed Daghi, and some cases, has caused the loss of the primary potassic alteration. The phyllic alteration in the bank of the Arpachai River has surrounded the potassic alteration in the form of a halo. In this alteration, feldspars and plagioclase have been replaced by sericite, clay minerals, and quartz, and in some cases, the rock has also lost its texture.

2.4.3. Hypogene argillic alteration

This alteration is one of the most extensive alterations in the area and shows a close association with epithermal-type mineralization. The mineralogical composition of this alteration is quartz, kaolinite, illite, and it is developed around the epithermal mineralization of the area and gradually turns into propylitic alteration. The origin of kaolinite (primary or secondary) cannot be determined due to deep weathering.

2.4.4. Supergene advanced argillic alteration

This alteration is developed along the fractures and waterways in some areas where sulfides, mainly pyrite, increase in the rocks. In some areas, especially near the peaks, the amount of pyrite in the rocks increases considerably, and this pyrite has no mineralization. The weathering of pyrite-rich rocks and mineralized areas along with the oxidation of sulfides has created sulfuric acid, and its effect on the rocks has caused this alteration. The main minerals of this alteration include kaolinite, illite, and gypsum. This alteration has deeply affected the hypogene alterations and sulfides on the surface so that primary alterations and sulfides cannot be identified.

2.4.5. Silica alteration

Silica alteration is one of the most significant alterations in the studied area. This alteration can be seen in two different forms.

2.4.5.1. Residual silica or vuggy quartz

This alteration is an indicator of high sulfide epithermal deposits, which is the result of the complete leaching of cations from rock by hydrothermal solutions with a pH of about 2. This alteration has occurred along fractures with a W-E trend, and it can be seen along the veins in zones with a width of several meters (2 to 5 meters).

2.4.5.2. Silica addition

This alteration is the addition of silica to the rock, and in most cases, it accompanies the alteration of residual silica. In some cases, samples of the region are completely composed of silica, and the amount of silica reaches more than 95%; This event is the result of the alteration of residual silica and the addition of silica. This alteration can be an excellent exploratory guide in the area.

2.4.6. Chlorite alteration

This alteration is recognized by the replacement of amphibole and pyroxene with calcite and chlorite and plagioclases with calcite and clay minerals. This alteration is often seen as halos around the alteration zones related to mineralization and has affected most of the rock units in the area.

2.5. Mineralization and alteration zoning pattern

In this study, in order to determine the geological model and alteration of the Masjed Daghi deposit, the logging data of the drilling cores of three exploratory boreholes (MAD1, MAD2, and MAD3) which were drilled in an east-west direction perpendicular to the Arpachai river were used. These boreholes have been drilled to the depths of 305, 408, and 385.30 meters, respectively. To investigate the type of mineralized rock unit and its alteration, 36 petrographic samples were collected and to study mineralization zones and ore composition, 24 mineralogical samples were taken from the drilling cores. Then, using the results of microscopic studies and logging of the cores, the geological model and alteration of the ore body have been determined. Masjed Daghi porphyry mineralization is related to an intrusive andesite-diorite porphyry volcanic system. Mineralogical studies and chemical analysis have shown that the mineralization in this complex is porphyry Cu-Au. In vertical direction, mineralization has occurred in both the volcanic unit (andesite) and the underlying subvolcanic body (porphyry diorite), but the main ore body is in the porphyry diorite unit. The main alteration associated with mineralization is potassic.

The MAD01 borehole begins with potassic alteration, so potassic alteration has limited outcrops at the surface. In the MAD02 borehole, potassic alteration starts at a depth of 52 m. From the surface to a depth of 43.1 meters is Alluvium and from 43.1 to 52 meters is argillic alteration (in the andesite unit). In the MAD03 borehole, the alteration from the surface to a depth of 34 m is argillic and the potassic type starts at 34 m. The phyllic alteration zone is not formed in this deposit. Only late-stage andesitic dykes exhibit Sercitic alteration. In terms of mineralization zones, the oxidation zone in these boreholes has a thickness of 49.7, 54 and 84 m, respectively, and the hypogene zone is located below it and extends to depths of more than 600 m. The supergene zone is not formed in this deposit (at least in the area of these three boreholes). The location of the porphyry diorite body is almost consistent with the axis of the Arpachai river. Because this body does not have much exposure on the surface, its dimensions are not known, but according to the limited drilling, it seems that its surface dimensions are about 400 meters in the east-west and 700 meters in the north-south direction. The geological, alteration, and mineralization model of Masjed Daghi deposit based on the studied boreholes is shown in Fig. 4.

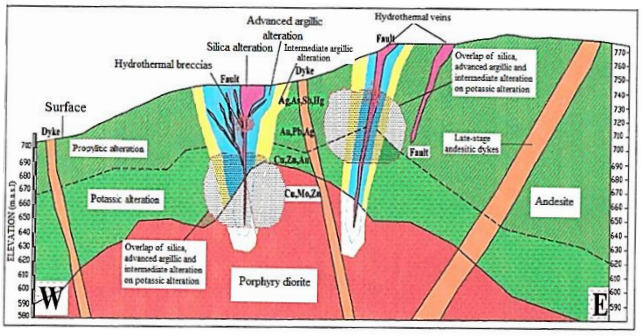

Fig. 4: The geological model, alteration, and mineralization of porphyry copper-epithermal gold in Masjed Daghi. It is necessary to explain that the potassic alteration zone extends in the depth direction in the porphyry diorite body [53].

2.6. Data set

According to the results of previous studies, the exploration area of Masjed Daghi was drilled for subsurface explorations and to complete existing surface information. A total of 16 exploratory boreholes with lengths between 72.6 and 195 m and a total of 1882 m were drilled by the National Iranian Copper Industries Company (NICICO). Four boreholes (BH8, BH9, BH11, and BH16) were drilled for the depth study of porphyry mineralization, and 12 boreholes were drilled for the depth study of vein epithermal mineralization (10 boreholes: BH1, BH2, BH3, BH4, BH5, BH6, BH7, BH13, BH14, and BH15) on the V_3 and two boreholes: BH10, BH12 on V_4 (Fig. 3). A total of 708 samples from boreholes have been taken and analyzed. The results of the laboratory analysis of the samples collected by the NICICO were provided to the authors of this article. In this study, we used the data from analyzing some boreholes for modelling both types of porphyry and epithermal mineralization. The information on the drilled exploratory boreholes is shown in Table 1.

3. Model description

First, a summary of the origin of the ANN and its applications is provided; then, we described the algorithms used for the ANN optimization.

3.1. Artificial neural network (ANN)

An ANN is a set of connections between units or nodes that try to function similarly to a set of neurons in the human brain [54]. The processing capability of the network originates from the type of connection between the units and the connection weights, which are either obtained from the learning process or are predetermined [55]. A neuron is the smallest information processing unit [56]. A layer is created from the community of several neurons that work in parallel. Each layer has a specific task, and by combining the layers, ANNs are built. According to the p Table 1: Specifications and coordinates of boreholes drilled in the study area.urpose for which the ANN is designed, several layers are considered [57]. An ANN is an information processing system created by simulating and simplifying the neural networks of the human body. Fig. 5 shows the general process of ANNs schematically. The output of other neurons is multiplied by different weights and reaches the new neuron as an input [58]. These inputs leave the neuron after being collected and passed through the transfer function (TF). Therefore, each neuron has a large amount of input and only one output. Connecting many of these neurons can form an ANN [59].

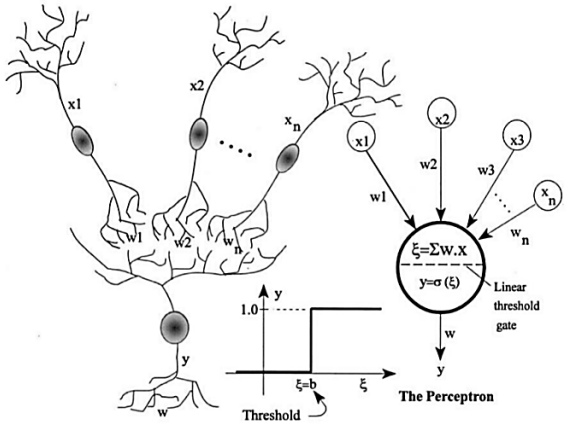

Fig. 5: The general trend of ANN schematically [60].

Table 1. Specifications and coordinates of boreholes drilled in the study area.

Hole ID	Depth(m)	Azimuth	Inclination	X(Easting)	Y(Northing)	Z(Elevation)	Number of boxes	Number of samples
BH1	110	10	15	581650	4303850	742	16	70
BH2	116	25	20	581686	4303831	745	18	70
BH3	105	10	15	581759	4303829	751	16	63
BH4	101	10	15	581913	4303776	775	17	65
BH5	85	15	10	581561	4303857	703	10	39
BH6	82	350	10	582179	4303776	770	13	25
BH7	100	350	10	582258	4303777	778	19	27
BH8	189	10	5	581520	4303931	702	25	83
BH9	140	10	15	581477	4304052	708	26	58
BH10	103.3	190	10	581733	4303268	751	20	18
BH11	195	25	20	581447	4303654	717	34	74
BH12	76.2	195	20	581934	4303427	758	13	20
BH13	72.9	0	25	582357	4303782	800	15	11
BH14	86	10	0	582074	4303786	778	15	18
BH15	163.3	350	10	582259	4303758	782	29	25
BH16	157.6	325	20	581464	4303775	700	29	42
Total	**1882**						**315**	**708**

*Coordinate format: UTM, Zone: 38S

3.2. Simulated annealing algorithm (SAA)

SAA is an algorithm for solving non-linear problems and is classified in the category of meta-heuristic algorithms. [61] which was first used in the 1980s [62, 63]. This algorithm is based on the Metropolis algorithm and relies on moving the thermodynamic system and reaching the system's equilibrium at minimum energy [64]. Later, other versions of this algorithm were used by researchers. [65, 66]. The beginning of the algorithm is to create an initial solution (x) and then another solution (y) is defined in the neighborhood of the initial solution randomly or based on a predefined relationship. The second generated solution (y) may be rejected or approved based on the Metropolis criterion, which, if approved, replaces the initial solution (x):

$$P = \begin{cases} 1, & \text{if } f(y) \le f(x) \\ e^{-\frac{(f(y)-f(x))}{t}}, & otherwise, \end{cases} \quad (1)$$

t is defined as temperature in the above relation. In 1993, Ingber examined the strengths and weaknesses of this algorithm in an article [68]. The flow chart of SAA is shown in the Fig. 6.

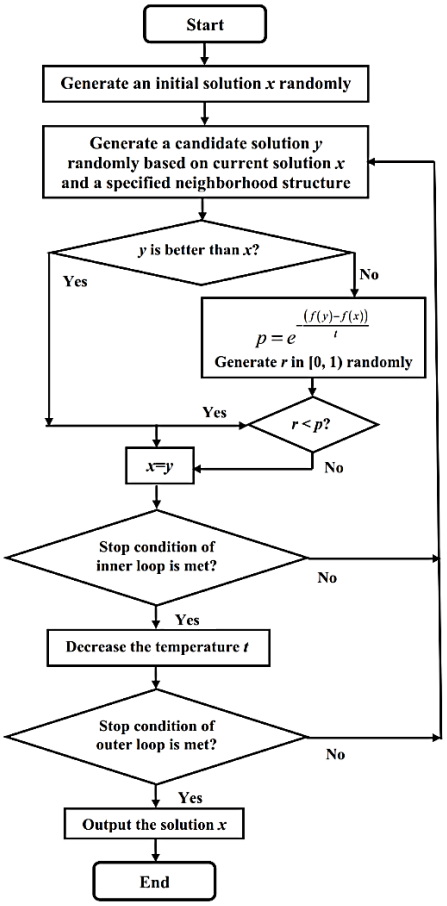

Fig. 6. Steps of the SAA performance.

3.3. Firefly algorithm (FA)

FA was introduced in late 2007 by Xin-She Yang and developed in 2010 [69]. The main idea of this algorithm is inspired by the optical communication between fireflies. This algorithm can be seen as a manifestation of swarm intelligence, in which a higher level of intelligence is created from the cooperation (and possibly competition) of simple and low-intelligence members, which certainly cannot be achieved by any of the components. The flow chart of the FA algorithm is shown in Fig. 7. For more details, you can refer to the relevant references [69].

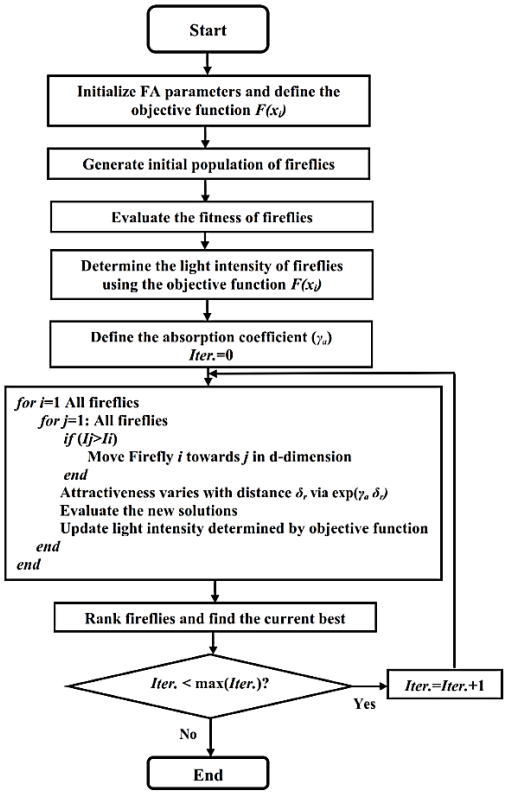

Fig. 7. Steps of the FA performance.

3.4. Invasive weed optimization algorithm (IWO)

IWO algorithm was proposed in 2006 by Mehrabian and Lucas in the form of an article [70]. The behavior of weeds in the way of reproduction is the basis of this algorithm. This algorithm lacks complexity, and diversity of parameters, and it is easy to create its execution program. Based on the principles of IWO, seeds are considered as possible solutions, and each seed represents a solution [71]. At first, several seeds are spread randomly as the initial answer in the search area. Each seed becomes a weed, and depending on each seed, it creates a different quality of weed. Newly generated weeds produce new weeds depending on their quality, and at each step, weeds with higher quality produce more weeds. This process continues until the best answer is reached [71].

The algorithm execution steps are as follows:

(a) Initialization: The initial population is randomly generated in the determined space of the problem.

(b) Reproduction: Depending on the fitness of each seed, several weeds will grow from each seed. The number of weeds produced is a linear function that increases from the minimum to the maximum possible value.

Spatial distribution: The production of new seeds is done around each seed with a specific standard deviation, normal distribution, and zero mean. The standard deviation from the initial value (δ_initial) decreases non-linearly until it reaches the final value (δ_final). As we become closer to the final steps, seeds are propagated with less scattering. The standard deviation in each step is calculated with the following equation:

$$\delta_{Iter_i} = \frac{(MaxIt-Iter_i)^{pow} \times (\delta_{initial}-\delta_{final})}{(MaxIt-1)^{pow}} + \delta_{final} \quad (2)[70]$$

(a) Competitive Exclusion: Because we can only advance a limited number of plants to the next step, there is competition between plants at each step and plants that do not produce seeds are removed from the cycle. The predetermined maximum number of plants (Pmax) is one of the parameters of the algorithm, which can be equal to the initial population. If the number of plants reaches the Pmax, the plants that did not produce the required seeds are removed and are not transferred to the next generation. The flow chart of the IWO algorithm is shown in Fig. 8.

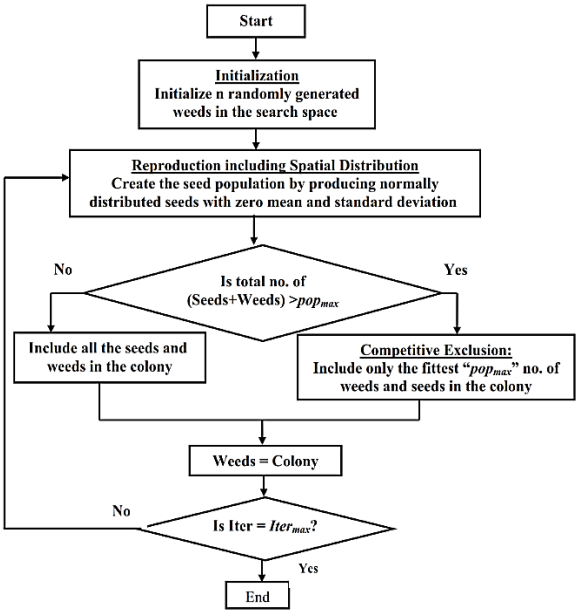

Fig. 8. The steps of the IWO algorithm performance.

3.5. Shuffled frog leaping algorithm (SFLA)

The shuffled Frog Leaping Algorithm (SFLA) is a meta-heuristic optimization algorithm developed by modelling the behavior of frogs. The initial version was introduced in 2003 and the discrete version in 2006. In 2009, an evolved version for solving continuous problems was presented by Zhen. The frog algorithm is an extended version of the Shuffled Complex Evolution (SCE) algorithm. The SCE algorithm is a combination of the genetic algorithm and the random search capability of the algorithm, which means controlled random search (CRS). For this reason, it can be placed in the category of memetic algorithms.

The SFLA is the same as the SCE algorithm with the difference that Elitism and Swarm Intelligence have been added to it.

Steps of the frog jump algorithm:

- First, the primary parameters are defined.
- The initial population (frogs) is generated randomly.
- The fitness of each member is calculated.
- All frogs are arranged in descending order based on their fitness.
- The frogs are divided into several groups (MemePlex) in such a way that the frog with the best competence is placed in the first group, the second frog in the second group, and the mth frog in the m group. In the same way, the m+1st frog is in the first group, as shown below [72]:

Frog individual: 1,2, ..., m, m+1, ...F

$$\text{n frogs}\left\{\begin{bmatrix}1\\m+1\\\vdots\\\vdots\end{bmatrix}\quad\begin{bmatrix}2\\m+2\\\vdots\\\vdots\end{bmatrix}\quad\dots\quad\begin{bmatrix}m\\2m\\\vdots\\F\end{bmatrix}\right. \tag{3}$$

1st memeplex 2nd memeplex m^{th} memeplex

- A local search is made to jump frogs with the worst fitness towards frogs with the best fitness. This mutation is according to relations 1 and 2 [73]:

$$\textit{Change in frog position } (D_i) = \textit{rand ()}.\ (X_b - X_w) \tag{4}$$

$$\textit{Change in frog position } (D_i) = \textit{rand ()}.\ (X_b - X_w) \tag{5}$$

In the above relationship, X_w and X_b are the frogs with the worst and best fitness in their group, respectively. D is the jump value of the weakest frog towards the best member of the group, $Dmax$ is the maximum allowable limit for frog jump, and rand is a random number between 0 and 1.

After applying the above changes, if the new frog has a better response than the worst frog in the group, it will be replaced. Otherwise, the same actions are repeated by replacing X_g with X_b. If a more suitable answer is not found by applying the above change, we will randomly generate an answer and replace it with the worst member of the group. This process continues for a specified number of times until the condition for finishing the algorithm is finally achieved. The flow chart of the SFLA algorithm is shown in the Fig. 9.

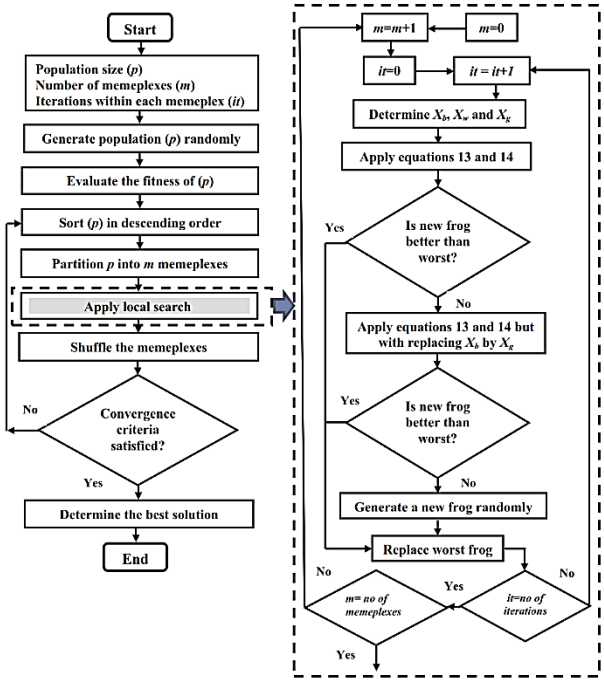

Fig.9. The steps of the SFLA performance.

4. The prediction of Cu and Au using ANN models

4.1. Inputs and outputs data

The prediction using the ANN model requires pre-processing, dividing the data into two categories of input and output, and then learning and testing the model which we address in this section.

In this study, the estimation of gold and copper with intelligent modelling is done separately for porphyry and epithermal mineralization. Copper estimation is conducted using data from exploratory boreholes drilled in porphyry mineralization, while gold estimation is performed using data obtained from epithermal mineralization. The inputs of the model are the same in both sections (Pb, Zn, Ag, Mo, and As), but the output of the porphyry section is copper and the output of the epithermal section is gold (Fig. 10).

4.2. Pre-processing of data

In modelling methods, before any calculation, the raw data is pre-processed; thus, the data are ready for modelling. In modelling with ANN, the data must first be normalized using a function. In this way,

the data are in the same range after normalization. Here, using the following function, all data are transformed in the range [-1,1]:

$$x_M = 2\left(\frac{x - x_{\min}}{x_{\max} - x_{\min}}\right) - 1 \quad (6)$$

where x represents the original raw data, x_M is the transformed value, and x_{min} (x_{max}) represents the minimum (maximum) raw data.

It should be noted that the model's outputs will be mapped to their corresponding real values by the inverse mapping function before calculating each performance measure. Before normalizing the data by the above function, the logarithmic transformation was applied to the initial raw data due to its non-normality. Because of the small amount of data (less than 1), the output of logarithmic transformation resulted in negative numbers. To overcome this problem, the data were first multiplied by 100, and then, the logarithmic transformation was applied to normalize the data. Therefore, in this study, the grade of the elements in the charts and tables is on a logarithmic scale.

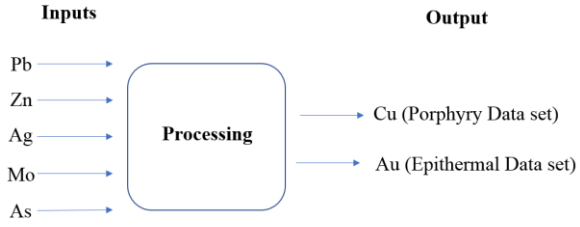

Fig. 10. The schematic of inputs and outputs of the model.

4.3. The parameters of the SAA, FA, IWO, and SFLA

To overcome some problems of ANNs, such as low learning speed and becoming stuck in local minima, it is helpful to use optimization algorithms for training ANNs. In the ANN, model training (the determination of weights and biases) is mainly done by the optimization algorithm. On the other hand, the structure of the model, including the number of hidden layers and the number of neurons can also be defined as an optimization problem and determined with the optimizer algorithm. Typically, optimization algorithms have parameters, such as maximum repetitions or the number of initial solutions, whose proper setting has a significant impact on the performance of the model. Here, using the obtained results, the model was built, as well as in other previous studies using these algorithms, and the algorithm parameters were adjusted. To achieve the appropriate structure of the model, during the execution of the program using different structures, these parameters were constant and did not change.

4.4. Evaluation criteria

Mean squared error (MSE), root mean squared error (RMSE), squared correlation coefficient (R^2), variance accounted for (VAF), and mean absolute percentage error (MAPE) were used to estimate the accuracy of the built model, where t_k is the measured value, $\hat{t}_k$ is the predicted value, and n is the number of samples. The equations of MSE, RMSE, R^2, VAF, and MAPE are given below [74]:

$$MSE = \frac{1}{n}\sum_{k=1}^{n}(t_k - \hat{t}_k)^2 \quad (7)$$

$$RMSE = \sqrt{\frac{1}{n}\sum_{k=1}^{n}(t_k - \hat{t}_k)^2} \quad (8)$$

$$R^2 = 1 - \frac{\sum_{k=1}^{n}(t_k - \hat{t}_k)^2}{\sum_{k=1}^{n} t_k^2 - \frac{\sum_{i=1}^{n}\hat{t}^2 k}{n}} \quad (9)$$

$$VAF = \left(1 - \frac{var(t_k - \hat{t}_k)}{var(t_k)}\right) \quad (10)$$

$$MAPE = \frac{1}{n}\sum_{k=1}^{n}\left|\frac{t_k - \hat{t}_k}{t_k}\right| \times 100 \quad (11)$$

5. Results

5.1. Modelling in porphyry mineralization

Data obtained from boreholes BH9, BH11, and BH16 were considered for modelling in porphyry mineralization. The results are shown in Tables 2-5. Also, the correlations and comparisons between the measured and predicted values for the training and testing datasets of the ANN-SAA model provided the best results compared to the rest of the models, as shown in Figs. 11 and 12. The transfer functions (TFs) used include tansig, logsig, and purelin abbreviated as T, L, and P, respectively.

5.2. Modelling in epithermal mineralization

Data obtained from boreholes (BH1, BH2, BH3, BH4, BH5, BH6, BH7, BH13, BH14, and BH15) on the V_3 vein and two boreholes (BH10, BH12) on the V_4 vein were considered for modelling in epithermal mineralization which the results are shown in the Tables 6-9. Also, the correlations and comparisons between the measured and predicted values for the training and testing datasets of the ANN-SAA model provided the best results compared to the rest of the models, as shown in Figs. 13 and 14. The TFs used include tansig, logsig, and purelin abbreviated as T, L, and P, respectively.

6. Discussion

The results obtained from modelling using different algorithms in this research showed that optimizing the model using SAA provides better results and lower modelling error. This result was obtained in both the porphyry and epithermal sections. The modelling results of copper prediction using porphyry data were better than those of gold prediction using epithermal data. Model execution was done using different sets of data (training and testing datasets). 10 different sets of the data were used and by comparing the results, the best category was chosen for running the model (Table 10). Moreover, to check the effectiveness of the results, the optimization was done using the BP algorithm and compared with the results obtained from the ANN-SAA model. The results show the better performance of ANN-SAA using the same data (Table 11).

Table 2. Some the ANN-SFLA model results (porphyry mineralization).

The structure of model	TF	mean squared error (MSE)		Squared correlation coefficient (R^2)	
		Train Data	Test Data	Train Data	Test Data
5-7-7-1	T-L-P	0.0642	0.0645	0.6081	0.6929
5-10-10-1	L-L-T	0.0651	0.0788	0.5902	0.5946
5-7-7-1	L-L-T	0.0595	0.0711	0.6335	0.6344
5-3-1	L-T	0.0707	0.0919	0.5557	0.5083
5-10-1	L-T	0.0559	0.0879	0.6495	0.6352
5-8-8-1	L-L-L	0.0625	0.0943	0.6106	0.4886
5-5-5-5-1	L-L-L-L	0.0901	0.1205	0.6065	0.6415
5-3-3-3-1	L-T-T-T	0.0672	0.0755	0.5812	0.6145
5-10-10-10-1	L-T-T-T	0.0589	0.0936	0.6603	0.4580
5-4-5-4-1	**L-T-L-T**	**0.0608**	**0.0632**	**0.6236**	**0.6974**

Table 3. Some the ANN-SAA model results (porphyry mineralization).

The structure of model	TF	mean squared error (MSE)		Squared correlation coefficient (R^2)	
		Train Data	Test Data	Train Data	Test Data
5-8-8-1	L-L-T	0.0393	0.0927	0.7699	0.5183
5-8-8-8-1	L-T-L-T	0.0579	0.1085	0.7931	0.5991
5-6-6-6-1	T-L-T-L	0.0799	0.1310	0.7213	0.5792
5-6-6-6-1	L-T-L-T	0.0485	0.0796	0.7428	0.6507
5-5-5-5-1	L-T-T-T	0.0517	0.0836	0.7237	0.6217
5-4-5-4-1	L-T-T-T	0.0455	0.0903	0.7321	0.5308
5-20-20-1	L-L-T	0.0829	0.1236	0.7976	0.5761
5-15-15-1	L-L-T	0.0294	0.0816	0.8212	0.5634
5-10-10-1	L-L-T	0.0589	0.0936	0.6603	0.4580
5-12-12-1	**L-L-T**	**0.0303**	**0.0371**	**0.8275**	**0.7357**

Table 4. Some the ANN-IWO model results (porphyry mineralization).

The structure of model	TF	mean squared error (MSE)		Squared correlation coefficient (R^2)	
		Train Data	Test Data	Train Data	Test Data
5-5-5-1	T-T-P	0.2417	0.4121	0.0906	0.2764
5-8-8-1	L-T-T	0.0998	0.1371	0.5270	0.4786
5-5-5-1	T-T-L	0.0878	0.1282	0.6855	0.6504
5-5-5-5-1	L-T-T-T	0.1058	0.1175	0.4676	0.6211
5-5-5-1	L-L-T	0.0948	0.1126	0.5515	0.5832
5-7-7-1	L-L-T	0.0934	0.1122	0.5835	0.4482
5-10-10-1	T-T-T	0.1631	0.2038	0.6170	0.5267
5-15-15-1	L-L-L	0.0813	0.1392	0.6301	0.4097
5-6-6-1	L-L-T	0.1506	0.1533	0.5108	0.3891
5-10-10-1	**L-L-T**	**0.0820**	**0.1071**	**0.5531**	**0.4327**

Table 5. Some the ANN- FA model results (porphyry mineralization).

The structure of model	TF	mean squared error (MSE)		Squared correlation coefficient (R^2)	
		Train Data	Test Data	Train Data	Test Data
5-7-1	T-T	0.1247	0.1475	0.5518	0.5049
5-7-7-1	T-L-T	0.0857	0.1424	0.6417	0.4826
5-15-1	L-T	0.1197	0.1716	0.6383	0.4412
5-12-1	L-T	0.0911	0.0909	0.6537	0.6410
5-9-1	L-T	0.0760	0.0930	0.6356	0.6400
5-5-5-5-1	L-T-T-T	0.0746	0.0969	0.6220	0.6512
5-5-5-5-1	L-T-L-T	0.0899	0.1329	0.6062	0.4220
5-6-6-1	L-T-T	0.0722	0.1043	0.5549	0.4303
5-8-8-1	L-L-T	0.0661	0.1352	0.6399	0.3149
5-6-6-1	**L-L-T**	**0.0610**	**0.0626**	**0.6166**	**0.6901**

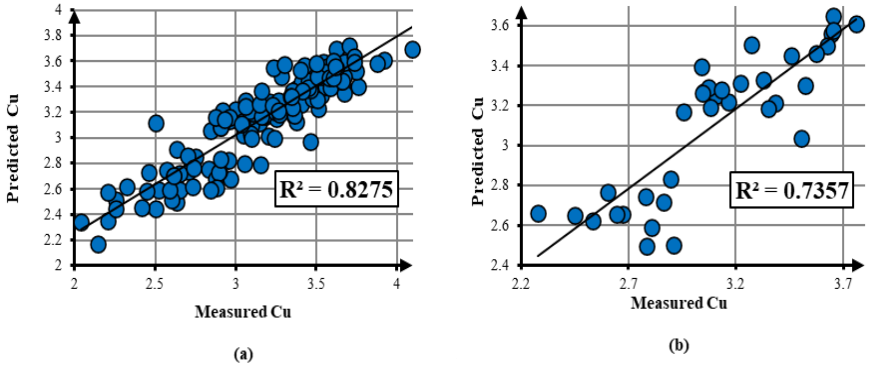

Fig. 11. Correlation between measured and predicted values of Cu (ANN-SAA). a) training dataset, b) testing dataset.

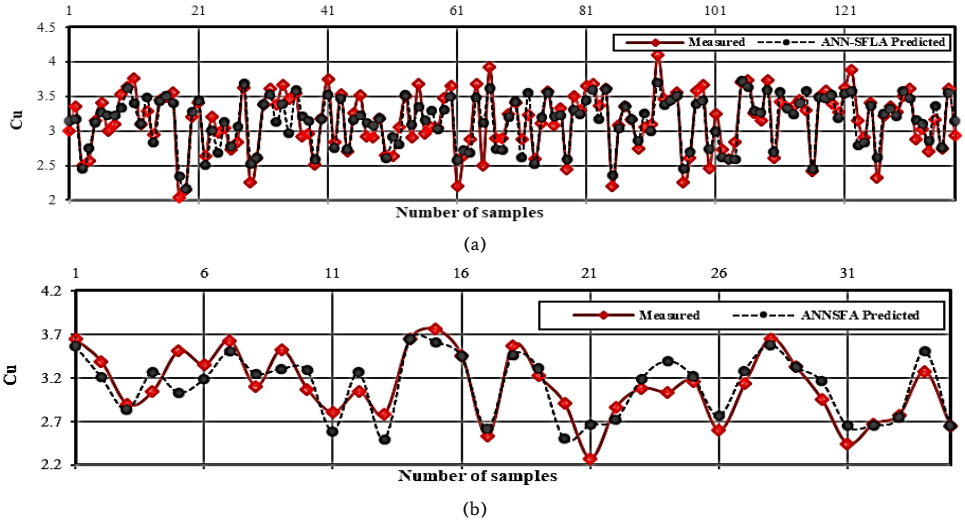

Fig. 12. Comparison between measured and predicted values of Cu (ANN-SAA). a) training dataset, b) testing dataset.

Table 6. Some the ANN- SFLA model results (epithermal mineralization).

The structure of model	TF	mean squared error (MSE)		Squared correlation coefficient (R^2)	
		Train Data	Test Data	Train Data	Test Data
5-8-8-1	L-L-T	0.0547	0.0436	0.5990	0.6857
5-5-5-1	L-L-T	0.0549	0.0402	0.5975	0.7128
5-6-3-1	L-L-T	0.0541	0.0426	0.6042	0.6889
5-8-8-1	L-L-L	0.0548	0.0439	0.6008	0.6853
5-10-10-10-1	L-T-T-T	0.0579	0.0442	0.5798	0.6895
5-6-6-6-1	L-L-L-T	0.0552	0.0449	0.5973	0.6711
5-8-8-8-1	L-L-L-T	0.0559	0.0448	0.5984	0.6839
5-15-1	L-T	0.0544	0.0395	0.6012	0.7110
5-8-1	L-T	0.0537	0.0392	0.6050	0.7130
5-10-1	**L-T**	**0.0536**	**0.0384**	**0.6056**	**0.7188**

Table 7. Some the ANN- SAA model results (epithermal mineralization).

The structure of model	TF	mean squared error (MSE)		Squared correlation coefficient (R^2)	
		Train Data	Test Data	Train Data	Test Data
5-3-3-3-1	L-T-T-T	0.0560	0.0467	0.6008	0.6742
5-8-8-8-1	L-T-T-T	0.0521	0.0450	0.6385	0.6931
5-5-5-5-1	L-T-T-T	0.0501	0.0398	0.6488	0.7284
5-6-6-6-1	L-T-T-P	0.0542	0.0482	0.6423	0.6955
5-5-5-5-1	L-T-L-T	0.0483	0.0446	0.6579	0.6823
5-8-8-1	L-L-T	0.0475	0.0466	0.6535	0.6531
5-11-11-1	L-L-L	0.0490	0.0472	0.6547	0.6703
5-10-10-1	L-T-T	0.0528	0.0424	0.6138	0.6808
5-15-15-1	L-L-T	0.0478	0.0529	0.5441	0.5992
5-11-11-1	**L-L-T**	**0.0463**	**0.0333**	**0.6713**	**0.7040**

Table 8. Some the ANN- IWO model results (epithermal mineralization).

The structure of model	TF	mean squared error (MSE)		Squared correlation coefficient (R^2)	
		Train Data	Test Data	Train Data	Test Data
5-15-15-1	L-L-T	0.0663	0.0517	0.5377	0.6210
5-10-10-1	L-L-T	0.0726	0.0594	0.5329	0.6529
5-7-7-1	L-L-T	0.0876	0.0828	0.5125	0.5927
5-8-3-1	L-L-T	0.0885	0.0809	0.3881	0.5191
5-5-5-1	L-L-T	0.0915	0.0881	0.5132	0.6002
5-5-5-5-1	L-T-T-T	0.1115	0.1163	0.4181	0.2259
5-15-1	L-T	0.1159	0.1197	0.5753	0.6488
5-10-1	L-T	0.0743	0.0433	0.5357	0.7024
5-5-1	L-T	0.0707	0.0618	0.5385	0.6215
5-8-1	**L-T**	**0.0679**	**0.0434**	**0.5142**	**0.6795**

Table 9. Some the ANN- FA model results (epithermal mineralization).

The structure of model	TF	mean squared error (MSE)		Squared correlation coefficient (R^2)	
		Train Data	Test Data	Train Data	Test Data
5-7-1	L-T	0.0687	0.0570	0.5737	0.6791
5-10-1	L-T	0.0643	0.0549	0.5437	0.6053
5-15-1	L-T	0.0942	0.0828	0.5598	0.6248
5-5-5-5-1	L-T-T-T	0.0692	0.0696	0.6262	0.6311
5-7-7-7-1	L-T-T-T	0.0658	0.0654	0.5994	0.6643
5-6-6-1	L-T-T	0.1221	0.1218	0.5726	0.6064
5-10-10-1	L-L-T	0.0590	0.0494	0.5836	0.6633
5-15-15-1	L-L-T	0.1010	0.1052	0.5672	0.6590
5-6-6-1	L-L-T	0.0881	0.0725	0.4873	0.6307
5-8-8-1	**L-L-T**	**0.0549**	**0.0405**	**0.6061**	**0.7157**

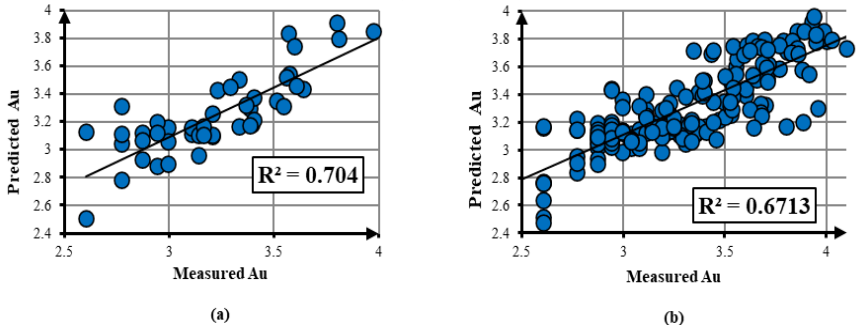

Fig. 13. Correlation between measured and predicted values of Au (ANN-SAA). a) training dataset, b) testing dataset.

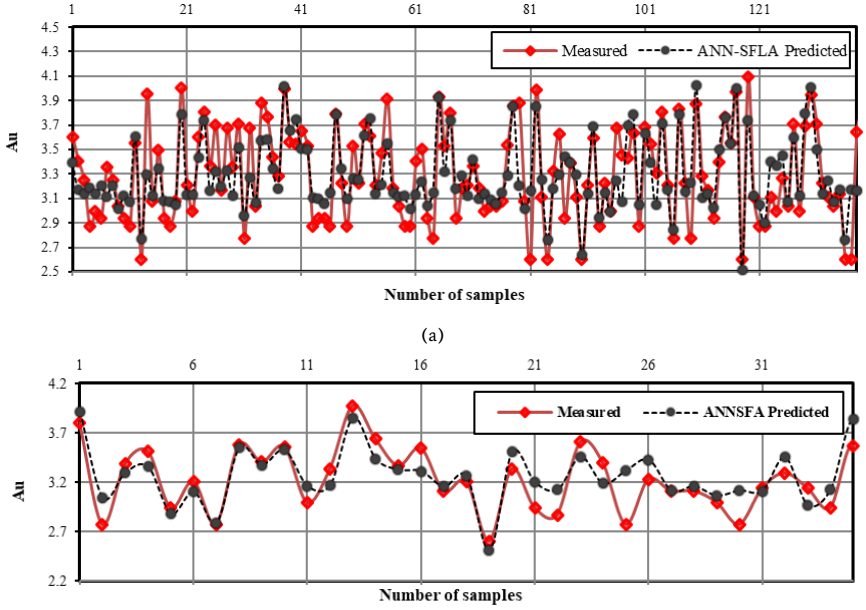

Fig. 14. Comparison between measured and predicted values of Au (ANN-SAA). a) training dataset, b) testing dataset.

Table 10. The performance of the models for predicting Cu and Au.

Description		R^2	MSE	RMSE	VAF	MAPE
ANN-SAA (Cu prediction)	Training	0.8275	0.0303	0.1741	0.8235	121.7
	Testing	0.7357	0.0371	0.1927	0.7293	409.6
ANN-SAA (Au prediction)	Training	0.6713	0.0463	0.2151	0.6702	107.9
	Testing	0.7040	0.0333	0.1824	0.7038	69.3

Table 11: The comparison of performance of the proposed models and ANN-BP model.

Description	Dataset	R^2		MSE	
		ANN-SAA	ANN-BP	ANN-SAA	ANN-BP
Cu prediction	Training	0.8275	0.7033	0.0303	0.0550
	Testing	0.7357	0.5357	0.0371	0.0777
Au prediction	Training	0.6713	0.6125	0.0463	0.1371
	Testing	0.7040	0.5835	0.0333	0.1950

7. Conclusions

In this research, an ANN was used for modelling with data obtained from exploratory drilling in two porphyry and epithermal mineralization of Masjed Daghi porphyry copper deposit in northwest Iran. The concentrations of gold and copper were predicted using this built model. The ANN optimization was performed using four optimization algorithms, including the SAA, FA, IWO, and SFLA and the following results were obtained:

- Among the optimization algorithms used to optimize the parameters of the ANN, the SAA provided better results.
- In this study, better results were obtained using the ANN-SAA model, both in the data of the porphyry mineralization and in the data of the epithermal mineralization of the deposit.
- The results of modelling using the ANN-SAA with the data of the porphyry part of the deposit to predict copper were better than the results of gold prediction using the data from the epithermal mineralization. Furthermore, R^2 and MSE of the ANN-SAA model for Cu prediction were 0.8275 and 0.0303 for training data, and 0.7357 and 0.0371 for testing data, respectively. Also, R^2 and MSE of the ANN-SAA model for Au prediction were 0.6713 and 0.0463 for training data, and 0.7040 and 0.0333 for testing data, respectively.
- Compared to the results of the ANN-BP model, the results of the ANN-SAA model mentioned in the previous paragraph provided better outcomes. Moreover, R^2 and MSE of the ANN-BP model for Cu prediction were 0.7033 and 0.0550 for training data, and 0.5357 and 0.0777 for testing data, respectively. Also, R^2 and MSE of the ANN-BP model for Au prediction were 0.6125 and 0.1371 for training data, and 0.5835 and 0.1950 for testing data, respectively.

The combined model of The ANN and optimization algorithms is a fast and cost-effective method for predicting the concentration of elements using related pathfinder elements that can be used in studies such as this.

REFERENCES

[1]. Hornik, K., M. Stinchcombe, and H. White, (1989). Multilayer feedforward networks are universal approximators. *Neural networks, 2(5),* 359-366. https://doi.org/10.1016/0893-6080(89)90020-8

[2]. Journel, A.G. and C.J. Huijbregts, (1978). Mining geostatistics, *Academic press*, Virginia, USA, 600 P.

[3]. Misra, D., et al., (2007). Evaluation of artificial neural networks and kriging for the prediction of arsenic in Alaskan bedrock-derived stream sediments using gold concentration data. *International Journal of Mining, Reclamation and Environment, 21(4),* 282-294. https://doi.org/10.1080/17480930701259294

[4]. Rendu, J. (1979), Kriging, logarithmic Kriging, and conditional expectation: comparison of theory with actual results, in Proc. 16th APCOM Symposium. Tucson, Arizona, 199-212.

[5]. Agterberg, F. and G. Bonham-Carter. (1999), Logistic regression and weights of evidence modeling in mineral exploration, in Proceedings of the 28th International Symposium on Applications of Computer in the Mineral Industry (APCOM), Colorado School of Mines, Colorado, USA, 483-490.

[6]. Porwal, A., et al., (2010). Weights-of-evidence and logistic regression modeling of magmatic nickel sulfide prospectivity in the Yilgarn Craton, Western Australia. *Ore Geology Reviews, 38(3),* 184-196. https://doi.org/10.1016/j.oregeorev.2010.04.002

[7]. Abedi, M., G.H. Norouzi, and N. Fathianpour, (2013). Fuzzy outranking approach: a knowledge-driven method for mineral prospectivity mapping. *International Journal of Applied Earth Observation and Geoinformation, 21(1),* 556-567. https://doi.org/10.1016/j.jag.2012.07.012

[8]. Abedi, M., S. Torabi, and G. Norouzi, (2013). Application of fuzzy AHP method to integrate geophysical data in a prospect scale, a case study: Seridune copper deposit. *Bollettino di Geofisica Teorica ed Applicata, 54(2),* 145-164. https://doi.org/10.4430/bgta0085

[9]. Afzal, P., et al., (2023). Mineral Resource Classification Using Geostatistical and Fractal Simulation in the Masjed Daghi Cu–Mo Porphyry Deposit, NW Iran. *Minerals, 13(3),* 370. https://doi.org/10.3390/min13030370

[10]. Daneshvar Saein, L., et al., (2022). Application of an improved zonality index model integrated with multivariate fractal analysis: epithermal gold deposits. *Geopersia, 12(2),* 379-394. https://doi.org/10.22059/geope.2022.339864.648652

[11]. Farhadi, S., et al., (2022). Combination of machine learning algorithms with concentration-area fractal method for soil geochemical anomaly detection in sediment-hosted Irankuh Pb-Zn deposit, Central Iran. *Minerals, 12(6),* 689. https://doi.org/10.3390/min12060689

[12]. Porwal, A., E.J.M. Carranza, and M. Hale, (2006). Bayesian network classifiers for mineral potential mapping. *Computers and Geosciences, 32(1),* 1-16.

[13]. Ziaii, M., A. Abedi, and M. Ziaei, (2009). Geochemical and mineralogical pattern recognition and modeling with a Bayesian approach to hydrothermal gold deposits. *Applied Geochemistry, 24(6),* 1142-1146. https://doi.org/10.1016/j.apgeochem.2009.02.006

[14]. Ghavami-Riabi, R., et al., (2010). U-spatial statistic data modeled on a probability diagram for investigation of mineralization phases and exploration of shear zone gold deposits. *Journal of Geochemical exploration, 104(1-2),* 27-33.

[15]. Mahdiyanfar, H. and M. Seyedrahimi-Niaraq, (2023). Integration of Fractal and Multivariate Principal Component Models for Separating Pb-Zn Mineral Contaminated Areas. *Journal of Mining and Environment, 14(3),* 1019-1035. 10.22044/jme.2023.13227.2424

[16]. Mahdiyanfar, H. and M. Seyedrahimi-Niaraq, (2024). Application of hybrid Wavelet-Fractal approach for denoising and spatial modeling of environmental pollution. *Journal of*

Mining and Environment, -. 10.22044/jme.2024.14197.2643

[17]. Seyedrahimi-Niaraq, M., H. Mahdiyanfar, and A.R. Mokhtari, (2022). Integrating principal component analysis and U-statistics for mapping polluted areas in mining districts. *Journal of Geochemical Exploration, 234,* 106924.

[18]. Brown, W.M., et al., (2000). Artificial neural networks: a new method for mineral prospectivity mapping. *Australian journal of earth sciences, 47(4),* 757-770.

[19]. Harris, D. and G. Pan, (1999). Mineral favorability mapping: a comparison of artificial neural networks, logistic regression, and discriminant analysis. *Natural Resources Research, 8(2),* 93-109. https://doi.org/10.1023/A:1021886501912

[20]. Harris, D., et al., (2003). A comparative analysis of favorability mappings by weights of evidence, probabilistic neural networks, discriminant analysis, and logistic regression. *Natural Resources Research, 12(4),* 241-255. https://doi.org/10.1023/B:NARR.0000007804.27450.e8

[21]. Lee, S., et al., (2014). A case study for the integration of predictive mineral potential maps. *Central European Journal of Geosciences, 6(3),* 373-392.

[22]. Leite, E.P. and C.R. de Souza Filho, (2009). Artificial neural networks applied to mineral potential mapping for copper-gold mineralizations in the Carajás Mineral Province, Brazil. *Geophysical Prospecting, 57(6),* 1049-1065. https://doi.org/10.1111/j.1365-2478.2008.00779.x

[23]. Leite, E.P. and C.R. de Souza Filho, (2009). Probabilistic neural networks applied to mineral potential mapping for platinum group elements in the Serra Leste region, Carajás Mineral Province, Brazil. *Computers & Geosciences, 35(3),* 675-687.

[24]. Oh, H.-J. and S. Lee, (2010). Application of artificial neural network for gold–silver deposits potential mapping: a case study of Korea. *Natural resources research, 19(2),* 103-124.

[25]. Rigol-Sanchez, J., M. Chica-Olmo, and F. Abarca-Hernandez, (2003). Artificial neural networks as a tool for mineral potential mapping with GIS. *International Journal of Remote Sensing, 24(5),* 1151-1156. https://doi.org/10.1080/0143116021000031791

[26]. Singer, D.A. and R. Kouda, (1996). Application of a feedforward neural network in the search for Kuroko deposits in the Hokuroku district, Japan. *Mathematical Geology, 28(8),* 1017-1023. https://doi.org/10.1007/BF02068587

[27]. Skabar, A. (2003), Mineral potential mapping using feed-forward neural networks, in Neural Networks, 2003. Proceedings of the International Joint Conference on: *IEEE*, 1814-1819.

[28]. Skabar, A., (2007). Mineral potential mapping using Bayesian learning for multilayer perceptrons. *Mathematical Geology, 39(5),* 439-451. https://doi.org/10.1007/s11004-007-9106-8

[29]. Skabar, A.A., (2005). Mapping mineralization probabilities using multilayer perceptrons. *Natural Resources Research, 14(2),* 109-123. https://doi.org/10.1007/s11053-005-6955-z

[30]. Dutta, S., et al., (2010). Machine learning algorithms and their application to Ore Reserve estimation of sparse and imprecise data. *Journal of Intelligent Learning Systems and Applications, 2(02),* 86.

[31]. Samanta, B., S. Bandopadhyay, and R. Ganguli, (2002). Data segmentation and genetic algorithms for sparse data division in Nome placer gold grade estimation using neural network and geostatistics. *Exploration and mining geology, 11(1-4),* 69-76. https://doi.org/10.2113/11.1-4.69

[32]. Samanta, B., S. Bandopadhyay, and R. Ganguli, (2006). Comparative evaluation of neural network learning algorithms for ore grade estimation. *Mathematical geology, 38(2),* 175-197. https://doi.org/10.1007/s11004-005-9010-z

[33]. Samanta, B., et al., (2004). Sparse data division using data segmentation and Kohonen network for neural network and geostatistical ore grade modeling in Nome offshore placer deposit. *Natural resources research, 13(3),* 189-200. https://doi.org/10.1023/B:NARR.0000046920.95725.1b

[34]. Abedi, M., G.H. Norouzi, and A. Bahroudi, (2012). Support vector machine for multi-classification of mineral prospectivity areas. *Computers and Geosciences, 46(1),* 272-283.

[35]. Li, X., Y. Xie, and Q. Guo. (2010), A new intelligent prediction method for grade estimation, in 7th International Symposium on Neural Networks, Shanghai University, China: *Springer*, 507-515.

[36]. Li, X.l., et al., (2013). Hybrid self-adaptive learning based particle swarm optimization and support vector regression model for grade estimation. *Neurocomputing, 118(1),* 179-190.

[37]. Zuo, R. and E.J.M. Carranza, (2011). Support vector machine: A tool for mapping mineral prospectivity. *Computers & Geosciences, 37(12),* 1967-1975.

[38]. Afzal, P., et al., (2022). Geochemical anomaly detection in the Irankuh District using Hybrid Machine learning technique and fractal modeling. *Geopersia, 12(1),* 191-199.

[39]. Brown, W., D. Groves, and T. Gedeon, (2003). Use of fuzzy membership input layers to combine subjective geological knowledge and empirical data in a neural network method for mineral-potential mapping. *Natural Resources Research, 12(3),* 183-200.

[40]. Porwal, A., E. Carranza, and M. Hale, (2004). A hybrid neuro-fuzzy model for mineral potential mapping. *Mathematical Geology, 36(7),* 803-826. https://doi.org/10.1023/B:MATG.0000041180.34176.65

[41]. Simpson, P.K., (1991). Artificial neural systems: foundations, paradigms, applications, and implementations, *McGraw-Hill, Inc.*209 P.

[42]. Toğan, V., (2012). Design of planar steel frames using teaching–learning based optimization. *Engineering Structures, 34,* 225-232.

[43]. Toğan, V., (2013). Design of pin jointed structures using teaching-learning based optimization. *Structural Engineering and Mechanics, An Int'l Journal, 47(2),* 209-225.

[44]. Uzlu, E., et al., (2014). Estimates of energy consumption in Turkey using neural networks with the teaching–learning-based optimization algorithm. *Energy, 75,* 295-303. https://doi.org/10.1016/j.energy.2014.07.078

[45]. Price, R.H. and S.J. Bauer, (1985), Analysis of the elastic and strength properties of Yucca Mountain tuff, Nevada, in 26th US Symposium on Rock Mechanics. United States. p. 89–96.

[46]. Hajihassani, M., et al., (2014). Prediction of airblast-overpressure induced by blasting using a hybrid artificial neural network and particle swarm optimization. *Applied Acoustics, 80,* 57-67.

[47]. Aghazadeh, M., et al., (2015). Temporal–spatial distribution and tectonic setting of porphyry copper deposits in Iran: constraints from zircon U–Pb and molybdenite Re–Os geochronology. *Ore geology reviews, 70,* 385-406.

[48]. Hassanpour, S., (2013). The alteration, mineralogy and geochronology (SHRIMP U–Pb and 40Ar/39Ar) of copper-bearing Anjerd skarn, north of the Shayvar Mountain, NW Iran. *International Journal of Earth Sciences, 102(3),* 687-699.

[49]. Jamali, H., et al., (2010). Metallogeny and tectonic evolution of

the Cenozoic Ahar–Arasbaran volcanic belt, northern Iran. *International Geology Review, 52(4-6),* 608-630.

[50]. Maghsoudi, A., et al., (2014). Porphyry Cu–Au mineralization in the Mirkuh Ali Mirza magmatic complex, NW Iran. *Journal of Asian Earth Sciences, 79,* 932-941. https://doi.org/10.1016/j.jseaes.2012.10.002

[51]. Imamalipour, A. and R. Mousavi, (2018). Vertical geochemical zonation in the Masjed Daghi porphyry copper-gold deposit, northwestern Iran: implications for exploration of blind mineral deposits. *Geochemistry: Exploration, Environment, Analysis, 18(2),* 120-131.

[52]. Ebrahimi, S., et al., (2017). Geology, mineralogy and ore fluid characteristics of the Masjed Daghi gold bearing veins system, NW Iran. *Journal of Economic Geology, 9(2),* 561-586. https://doi.org/10.22067/econg.v9i2.51493

[53]. Imamalipour, A., et al., (2011). Geological, Alteration and magnetic anomaly pattern of Masjeddaghi porphyry copper deposit (East of Julfa). *Advanced Applied Geology, 1(2),* 77-89.

[54]. Jorjani, E., S.C. Chelgani, and S. Mesroghli, (2008). Application of artificial neural networks to predict chemical desulfurization of Tabas coal. *Fuel, 87(12),* 2727-2734.

[55]. Monjezi, M. and H. Dehghani, (2008). Evaluation of effect of blasting pattern parameters on back break using neural networks. *International Journal of Rock Mechanics and Mining Sciences, 45(8),* 1446-1453.

[56]. Specht, D.F., (1991). A general regression neural network. *IEEE Transactions on Neural Networks, 2(6),* 568-576.

[57]. Acharya, C., et al., (2006). Prediction of sulphur removal with Acidithiobacillus sp. using artificial neural networks. *Ecological modelling, 190(1),* 223-230.

[58]. Ardebili, P. N., Jozanikohan, G., and Moradzadeh, A. (2024). Estimation of porosity and volume of shale using artificial intelligence, case study of Kashafrud Gas Reservoir, NE Iran. *Journal of Petroleum Exploration and Production Technology*, *14*(2), 477-494.

[59]. Hagan, M.T., H.B. Demuth, and M.H. Beale, (1996). Neural network design, *PWS Publishing Co*, Boston London.

[60]. Basheer, I.A. and M. Hajmeer, (2000). Artificial neural networks: fundamentals, computing, design, and application. *Journal of microbiological methods, 43(1),* 3-31. https://doi.org/10.1016/S0167-7012(00)00201-3

[61]. Assad, A. and K. Deep, (2018). A hybrid harmony search and simulated annealing algorithm for continuous optimization. *Information Sciences, 450,* 246-266.

[62]. Černý, V., (1985). Thermodynamical approach to the traveling salesman problem: An efficient simulation algorithm. *Journal of optimization theory and applications, 45(1),* 41-51.

[63]. Kirkpatrick, S., C.D. Gelatt Jr, and M.P. Vecchi, (1983). Optimization by simulated annealing. *science, 220(4598),* 671-680.

[64]. Metropolis, N., et al., (1953). Equation of state calculations by fast computing machines. *The journal of chemical physics, 21(6),* 1087-1092.

[65]. Xinchao, Z., (2011). Simulated annealing algorithm with adaptive neighborhood. *Applied Soft Computing, 11(2),* 1827-1836. https://doi.org/10.1016/j.asoc.2010.05.029

[66]. García-Martínez, C., M. Lozano, and F.J. Rodríguez-Díaz, (2012). A simulated annealing method based on a specialised evolutionary algorithm. *Applied Soft Computing, 12(2),* 573-588.

[67]. Fattahi, H. and H. Bazdar, (2017). Applying improved artificial neural network models to evaluate drilling rate index. *Tunnelling and Underground Space Technology, 70,* 114-124.

[68]. Ingber, L., (1993). Simulated annealing: Practice versus theory. *Mathematical and computer modelling, 18(11),* 29-57.

[69]. Yang, X.-S., (2010). Nature-inspired metaheuristic algorithms, *Luniver press*.

[70]. Mehrabian, A.R. and C. Lucas, (2006). A novel numerical optimization algorithm inspired from weed colonization. *Ecological informatics, 1(4),* 355-366. https://doi.org/10.1016/j.ecoinf.2006.07.003

[71]. Zhou, Y., et al., (2015). A discrete invasive weed optimization algorithm for solving traveling salesman problem. *Neurocomputing, 151,* 1227-1236.

[72]. Maaroof, B.B., et al., (2022). Current studies and applications of shuffled frog leaping algorithm: a review. *Archives of Computational Methods in Engineering, 29(5),* 3459-3474.

[73]. Elbeltagi, E., T. Hegazy, and D. Grierson, (2007). A modified shuffled frog-leaping optimization algorithm: applications to project management. *Structure and Infrastructure Engineering, 3(1),* 53-60.

[74]. Chicco, D., M.J. Warrens, and G. Jurman, (2021). The coefficient of determination R-squared is more informative than SMAPE, MAE, MAPE, MSE and RMSE in regression analysis evaluation. *Peerj computer science, 7,* e623.